Symbolic Nodal Analysis of Analog Integrated Circuits Using Pathological Elements

E. Tlelo-Cuautle
Department of Electronics
INAOE, México
Email: etlelo@inaoep.mx

C. Sánchez-López
Faculty of Basic Sciences and Technology
Universidad Autónoma de Tlaxcala, México
Email: carlsan@ieee.org

Sheldon X.-D. Tan
Department of Electrical Engineering
University of California at Riverside
Email: stan@ee.ucr.edu

***Abstract*— Improvements in analog signal processing applications require the selection of adequate active devices. However, each kind of active device offers different port-characteristics. For instance, the parasitic elements play an important role in selecting the best one for a given application. Symbolic nodal analysis is a useful tool to derive electrical characteristics of analog circuits, but compact models for the active devices are required to generate small matrices and analytical expressions. That way, this paper shows the usefulness of using pathological elements to generate behavioral models including dominant parasitic elements. The proposed approach is useful for the selection of active devices in analog design and synthesis procedures.**

I. Introduction

Analog integrated circuits (ICs) encounter applications in signal amplification, filtering, data acquisition systems, sensor conditioning, biomedical implants, actuator conditioning, oscillators, mixers and so on [1]. Those applications are possible thanks to the availability of a huge plethora of active devices [2], [3], [4], and thanks to the appropriate exploitation of their electrical characteristics. However, improvements in analog signal processing applications require the selection of adequate active devices. This is a pretty difficult task, because each kind of active device offers different port-characteristics, so that parasitic elements play an important role in selecting the best one for a given application. Fortunately, symbolic nodal analysis has demonstrated to be a useful tool to derive behavioral expressions of analog ICs [1], [2], [4], [5], [6], [7]. The formulated equations are easily solved by applying determinant decision diagrams (DDDs) [2], [7], [8], [9], [10], and parallel simulations accelerate time computation when deriving exact symbolic expressions [11]. However, compact models for the active devices are required to generate small matrices and to derive simplified analytical expressions. That way, this paper shows the usefulness of using pathological elements to generate behavioral models including dominant parasitic elements for the selection of active devices in design and synthesis procedures [1], [3], [6], [7].

II. Symbolic Nodal Analysis

In performing symbolic analysis one should be aware that by using detailed models of active devices, the generated expressions can be too large, while by using compact models the expression may be very compact or reduced. In both cases, the generated symbolic expression approximates the exact response with some error tolerance [1], [4], [7].

When applying symbolic nodal analysis techniques, the use of active device models based on nullors and/or pathological elements has demonstrated advantages in the formulation of small and sparse matrices [2], [7], [9], [10]. In addition, models based on nullors and/or pathological elements also allows us to include parasitic circuit elements [4], such as input and output impedances and gain [5]. Additionally, symbolic nodal analysis of nullor and/or pathological circuits can also be applied to perform noise [9] and sensitivity analysis [10].

In short, as demonstrated in [2], when applying traditional modified nodal analysis (MNA) [7], the formulated system of symbolic equations is bigger than by applying nodal analysis to nullor and/or pathological circuits. This is again highlighted herein by analyzing a universal filter consisting of current followers with multiple outputs, where each current follower can be modeled by a current controlled current source (CCCS) or by nullors and/or pathological elements. In the former case one should apply MNA and each CCCS augments one order (column and row) to the admittance matrix, while a nullor and/or pathological model neither reduces nor augments the order. This is described in the following section.

III. Modeling using Pathological Elements

Mixed-mode active devices process voltages and currents among their ports, and they can be modeled by using nullors as the illustrative examples presented in [4] for current conveyors and the CFOA. However, when they have inverting properties, more compact models can be generated by using the pathological voltage mirror and/or pathological current mirror elements [2].

As unity-gain cells [3], the voltage mirror and current mirror can be modeled by using nullors with independent gain, input and output impedances, as already shown in [5]. The nullor-equivalent of the current mirror is very useful in formulating a reduced system of equations, as demonstrated in [1] through performing symbolic nodal analysis of an all-pole third-order low-pass filter implemented with dual-output current mirrors.

Lets us consider the dual-output current follower (DOCF) diagram shown in Fig. 1. It can also be called dual-output current mirror (DOCM). The difference is that as a DOCF, i_z+ stands for a positive current follower (CF+) which is

978-1-4673-0859-5/12/$31.00 ©2012 IEEE

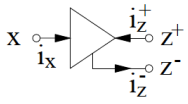

Fig. 1. Dual-output current follower taken from [12].

synonymous of the current mirror, and i_z- stands for a negative current follower (CF-) which can be obtained by cascading two current mirrors, as shown in [3]. As a DOCM, i_z+ stands for a current mirror, and i_z- stands for a current follower which can be implemented by the cascade connection of two current mirrors.

The model of this DOCF can be derived by using two current-controlled current sources (CCCSs), as shown in Fig. 2. As one sees, that model includes the parasitic input resistance R_{in} (ideally zero), the gains α for i_z+ and β for i_z-, and the output resistances R_oz+ and Ro_z- (ideally ∞). However, using this model in the MNA formulation, each CCCS augments one order (col and row) to the admittance matrix [7]. This is a drawback which is solved by using a model composed of nullors and/or pathological elements [2].

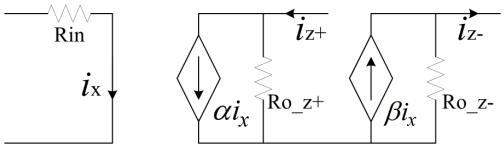

Fig. 2. CCCS-based model of the DOCF shown in Fig. 1.

The nullor-equivalent of the DOCF is shown in Fig. 3. That model includes the parasitic input impedance Z_{in} (ideally zero), the gains denoted by $1/A_z+$ (α in Fig. 2) for i_z+ and $1/A_z-$ (β in Fig. 2) for i_z-, and the output impedances Z_oz+ and Z_oz- (ideally ∞). Regarding the current output for i_z+, this model is not only quite useful in performing symbolic nodal analysis, but also has the advantage of not augmenting the order in the admittance matrix formulation [1]. However, regarding the current output for i_z-, this model for the DOCF is similar to that one by using CCCSs.

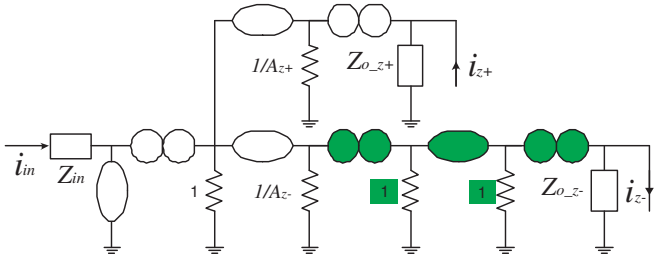

Fig. 3. Nullor-equivalent of the DOCF already introduced in [5].

We introduce here the model shown in Fig. 4. As one sees, it is an improved version of Fig. 3, where the two green-norators, the two unitary green-resistors and the green-nullator are replaced by the pathological current mirror element, while

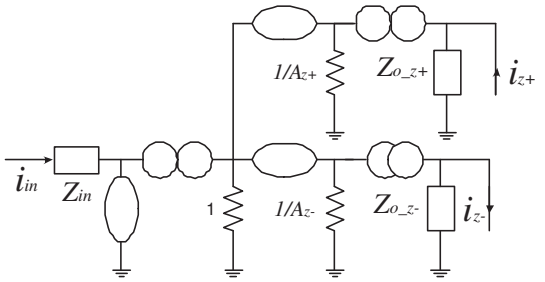

Fig. 4. DOCF modeled by nullors and the pathological current mirror.

the non-ideal gains and impedances remain intact. This new model does not augment the order of the admittance matrix formulation, as it does when using the CCCS-based model in the MNA formulation, as discussed above. Moreover, the pathological current mirror element is quite useful to derive compact models for current conveyors and other mixed-mode active devices, as already shown in [2]. The pathological voltage mirror element is the adjoint of the pathological current mirror and it is also quite useful in modeling active devices with voltage inverting properties [2], [4], [5], [7].

IV. Deriving Analytical Expressions in a Universal Filter

Lets us consider the universal active filter shown in Fig. 5. It consists of one current follower (CF-) to measure the high-pass filter response, one DOCF where the positive output (i_z+) is used to measure the band-pass response, and one three-outputs current follower (TOCF) where one negative output (i_z-) is used to measure the low-pass response.

If the MNA formulation is performed, using the CCCS-based model the admittance matrix will have size 17×17, because the circuit has 8 nodes (a,b,c,d,e, and f,g,h are added through connecting one resistor to each output to measure the filter responses in Fig. 6), 3 nodes are added to include the parasitic input resistance R_{in} to each CF, and 6 rows and cols are added for the 6 CCCSs (1 for the CF-, 2 for the DOCF and 3 for the TOCF).

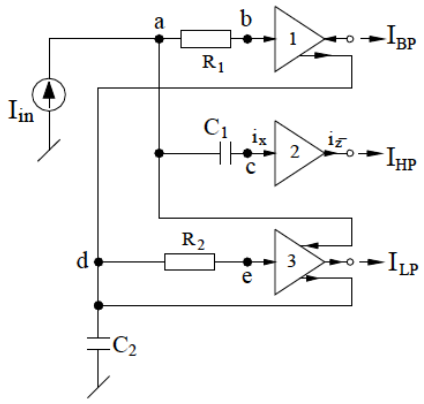

Fig. 5. Universal filter composed of multiple-outputs current mirrors [12].

If we use the derived pathological-equivalent model shown in Fig. 6, the admittance matrix will have size 11×11, because the circuit has 8 nodes (a,b,c,d,e,f,g,h), and only 3 nodes are added to include the parasitic input resistance R_{in} to each CF. That is, from the properties of the nullator, norator and pathological current mirror element described in [2], [4], [5], [7], the 12 nodes labeled from 1 to 12 and colored in green in Fig. 6 are reduced to 3, because we have 12 nodes minus 5 nullator-norator pairs, and minus 4 nullator-pathological current mirror pairs, leading to 12-5-4=3. The formulated system of equations by applying symbolic nodal analysis is given in (1). Note that the three CFs have the same $R_{in}, R_{ozp}, R_{ozn}, A_{zp}$, and A_{zn}, but they can be different in general. Ideally, the gains are unitary, then input resistance is zero and the output resistance is ∞.

The exact solution to (1), for the three output characteristics I_{BP}, I_{HP} and I_{LP}, has the same denominator given by (3). As one sees, the parasitic elements and the gains are included.

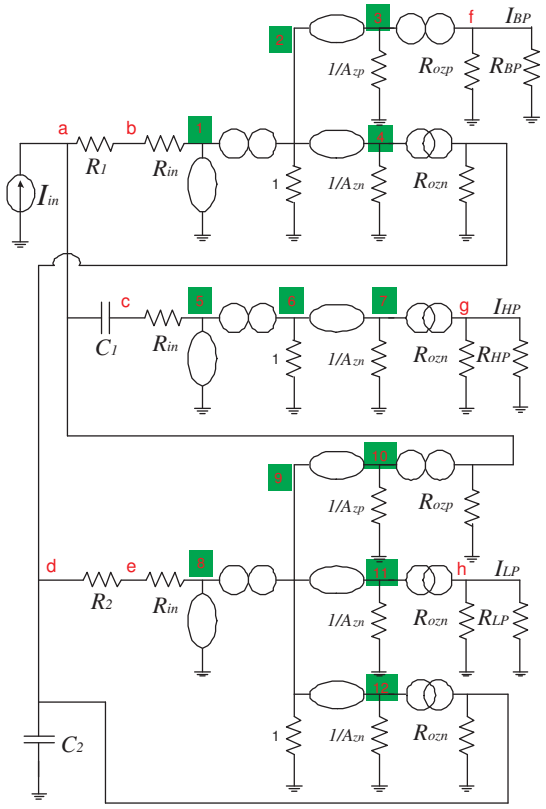

Fig. 6. Pathological equivalent of the universal filter.

where,

$$i = \begin{bmatrix} I_{in} \\ 0 \\ 0 \\ 0 \\ 0 \\ 0 \\ 0 \\ 0 \\ 0 \\ 0 \\ 0 \end{bmatrix} \qquad v = \begin{bmatrix} v_a \\ v_b \\ v_c \\ v_d \\ v_e \\ v_f \\ v_g \\ v_h \\ v_{2,3,4} \\ v_{6,7} \\ v_{9,10,11,12} \end{bmatrix} \tag{2}$$

$$\begin{aligned}\Delta = &(sg_{in}^3C_2g_{ozp} + g_1sg_{in}^2C_2g_{ozp} + s^2C_1g_{in}^2C_2g_{ozp} + \\ &g_1s^2C_1g_{in}C_2g_{ozp} + 2g_{in}^3g_{ozn}g_{ozp} + 2g_1g_{in}^2g_{ozn}g_{ozp} + \\ &2sC_1g_{in}^2g_{ozn}g_{ozp} + 2g_1sC_1g_{in}g_{ozn}g_{ozp} + g_{in}^3g_2g_{ozp} + \\ &g_1g_{in}^2g_2g_{ozp} + sC_1g_{in}^2g_2g_{ozp} + g_1sC_1g_{in}g_2g_{ozp} + sg_2g_1g_{in}^2C_2 \\ &+s^2C_1g_2g_{in}^2C_2 + 2s^2C_1g_2g_1g_{in}C_2 + 2g_2g_1g_{in}^2g_{ozn} + \\ &2sC_1g_2g_{in}^2g_{ozn} + 4sC_1g_2g_1g_{in}g_{ozn} - g_2g_1g_{in}^3A_{zn} - \\ &sC_1g_2g_{in}^3A_{zn} - 2sC_1g_2g_1g_{in}^2A_{zn} + sg_2g_{in}^2C_2g_{ozp} + \\ &sg_2g_1g_{in}C_2g_{ozp} + s^2C_1g_2g_{in}C_2g_{ozp} + s^2C_1g_2g_1C_2g_{ozp} + \\ &2g_2g_{in}^2g_{ozn}g_{ozp} + 2g_2g_1g_{in}g_{ozn}g_{ozp} + 2sC_1g_2g_{in}g_{ozn}g_{ozp} + \\ &2sC_1g_2g_1g_{ozn}g_{ozp} - g_2g_{in}^3A_{zn}g_{ozp} - g_2g_1g_{in}^2A_{zn}g_{ozp} - \\ &sC_1g_2g_{in}^2A_{zn}g_{ozp} - sC_1g_2g_1g_{in}A_{zn}g_{ozp} + sC_1g_2g_1g_{in}^2A_{zn}A_{zp} \\ &+g_2g_1g_{in}^3A_{zn}A_{zp} + g_1sg_{in}^3C_2 + s^2C_1g_{in}^3C_2 + 2g_1s^2C_1g_{in}^2C_2 \\ &+2g_1g_{in}^3g_{ozn} + 2sC_1g_{in}^3g_{ozn} + 4g_1sC_1g_{in}^2g_{ozn} + g_1g_{in}^3g_2 + \\ &sC_1g_{in}^3g_2 + 2g_1sC_1g_{in}^2g_2)(g_{ozp} + g_{BP})(g_{ozn} + g_{HP})(g_{ozn} + g_{LP})\end{aligned} \tag{3}$$

In the ideal case: $R_{in} = 0, R_{ozp} = R_{ozn} = \infty, A_{zp} = 1$, and $A_{zn} = 1$. Besides, taken into account $R_{in} \neq 0$ the reduced denominator is given by

$$\begin{aligned}\Delta_{ideal} = &(s^2C_1C_2 + g_1g_2 + g_1sC_2)g_{BP}g_{HP}g_{LP}g_{in}^3 + \\ &(sg_2g_1C_2 + s^2C_1g_2C_2 + sC_1g_2g_1 + 2g_1s^2C_1C_2)g_{BP}g_{HP}g_{LP}g_{in}^2 \\ &+2s^2C_1g_2g_1C_2g_{BP}g_{HP}g_{LP}g_{in}\end{aligned} \tag{4}$$

Solving for the Low-Pass response, i.e. $I_{LP} = g_{LP}v_h$, we first compute v_h which is given by (5), and includes R_{in}. Afterwards, the final expression with R_{in}=0 is given by (6). In the same way, the ideal filter characteristics for the band-pass and high-pass responses are given by (7) and (8). Noise and sensitivity analysis can be performed by applying [9], [10].

$$v_h = I_{in}g_1g_2g_{BP}g_{HP}g_{in}^3 + I_{in}sC_1g_1g_2g_{BP}g_{HP}g_{in}^2/\Delta_{ideal} \tag{5}$$

$$\frac{I_{LP}}{I_{in}} = \frac{g_1g_2/C_1C_2}{s^2 + sg_1/C_1 + g_1g_2/C_1C_2} \tag{6}$$

$$\frac{I_{BP}}{I_{in}} = \frac{sg_1/C_1}{s^2 + sg_1/C_1 + g_1g_2/C_1C_2} \tag{7}$$

$$\frac{I_{HP}}{I_{in}} = \frac{s^2}{s^2 + sg_1/C_1 + g_1g_2/C_1C_2} \tag{8}$$

$$[I] = \begin{bmatrix} g_1 + sC_1 + g_{ozp} & -g_1 & -s*C_1 & 0 & 0 & 0 & 0 & 0 & 0 & 0 & A_{zp} \\ -g_1 & g_1 + g_{in} & 0 & 0 & 0 & 0 & 0 & 0 & 0 & 0 & 0 \\ -sC_1 & 0 & sC_1 + g_{in} & 0 & 0 & 0 & 0 & 0 & 0 & 0 & 0 \\ 0 & 0 & 0 & 2g_{ozn} + g_2 + sC_2 & -g_2 & 0 & 0 & 0 & -A_{zn} & 0 & -A_{zn} \\ 0 & 0 & 0 & -g_2 & g_2 + g_{in} & 0 & 0 & 0 & 0 & 0 & 0 \\ 0 & 0 & 0 & 0 & 0 & g_{ozp} + g_{BP} & 0 & 0 & -A_{zp} & 0 & 0 \\ 0 & 0 & 0 & 0 & 0 & 0 & g_{ozn} + g_{HP} & 0 & 0 & -A_{zn} & 0 \\ 0 & 0 & 0 & 0 & 0 & 0 & 0 & g_{ozn} + g_{LP} & 0 & 0 & -A_{zn} \\ 0 & -g_{in} & 0 & 0 & 0 & 0 & 0 & 0 & 1 & 0 & 0 \\ 0 & 0 & -g_{in} & 0 & 0 & 0 & 0 & 0 & 0 & 1 & 0 \\ 0 & 0 & 0 & 0 & -g_{in} & 0 & 0 & 0 & 0 & 0 & 1 \end{bmatrix} [v] \tag{1}$$

The current-feedback opamp (CFOA) is another active device quite useful in linear and nonlinear applications [1], [3], [7]. It has four ports as shown in Fig. 7(a), and basically, it can be designed by cascading a positive-type second generation current conveyor (CCII+) with a voltage follower (VF) [3]. That way, its nullor-equivalent is shown in Fig. 7(b) [4]. One can identify the topology associated to the pathological current mirror colored in green from Fig. 3. Besides, by using the pathological current mirror element, its compact model is shown in Fig. 8 [2], where the dominant parasitics are included. In a similar manner, other kinds of active devices, especially the multiple outputs current conveyors [2], [4], can be modeled by using nullors and the pathological current mirror element.

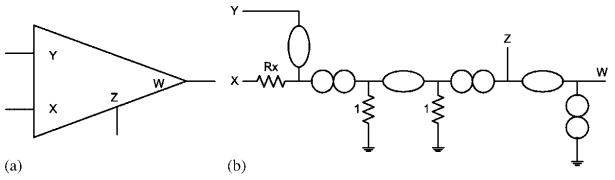

Fig. 7. (a) CFOA description, and its (b) nullor-equivalent including R_x [4].

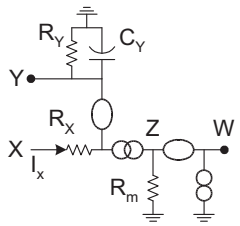

Fig. 8. Pathological-equivalent of the CFOA including parasitics [2].

Another illustrative example is the current-mode active filter shown in Fig. 9. It consists of 5 DOCFs (CM2-CM6, all with positive outputs) and one current mirror (CM1). If assumming all the current mirros to include their input resistance ($R_i = 1/g_i$), by applying symbolic nodal analysis [2], the admittance matrix has size 7×7, while the MNA formulation becomes 18×18 (7 nodes + 11 stamps for the CCCSs).

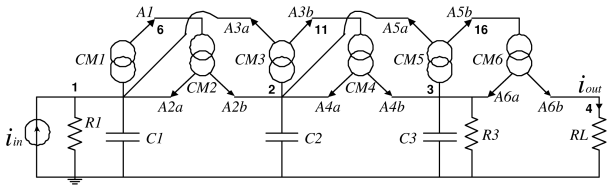

Fig. 9. All-pole low-pass filter implemented with DOCMs [1].

The derived symbolic expression becomes,

$$\frac{i_{out}}{i_{in}} = \frac{g_i^6}{\left(C_2 {g_i}^3 C_3 g_1 + C_2 {g_i}^3 g_3 C_1\right) s^2 + \left({g_i}^5 C_3 + {g_i}^5 C_1 + C_2 {g_i}^3 g_3 g_1\right) s + {g_i}^5 g_1 + {g_i}^5 g_3 + C_2 {g_i}^3 C_3 C_1 s^3} \quad (9)$$

Other illustrative examples for transistor-based amplifiers and oscillator can be found in [1], [7].

V. Conclusion

This paper highlighted the usefulness of using the pathological current mirror element to model several active devices, such as: current mirrors/followers, CFOAs and current conveyors. The main advantage of those derived models relies on the application of symbolic nodal analysis to formulate smaller matrices compared to traditional MNA formulation.

The proposed models based on pathological elements also allows us to include parasitic elements, so that the derived behavioral models capture the real behavior of the active devices. As a result, the proposed modeling approach is quite useful to perform symbolic nodal analysis of analog circuits, while the derived analytical expressions can be used to improve synthesis and/or optimization procedures.

Acknowledgment

This work is supported by UC MEXUS-CONACYT CN-11-575, and by CONACyT/Mexico 131839-Y.

References

[1] E. Tlelo-Cuautle, *Integrated Circuits for Analog Signal Processing*, Springer-Verlag, 2012

[2] C. Sánchez-López, F.V. Fernández, E. Tlelo-Cuautle, S. X.-D. Tan, Pathological Element-Based Active Device Models and Their Application to Symbolic Analysis, *IEEE Transactions on Circuits and Systems I: Regular papers*, vol. 58, no. 6, pp. 1382-1395, 2011.

[3] M.A. Duarte-Villaseñor, E. Tlelo-Cuautle, L. Gerardo de la Fraga, Binary genetic encoding for the synthesis of mixed-mode circuit topologies, *Circuits, Systems and Signal Processing*, vol. 31, no. 3, pp. 849-863, 2012.

[4] E. Tlelo-Cuautle, C. Sánchez-López, D. Moro-Frias, Symbolic analysis of (MO)(I)CCI(II)(III)-based analog circuits, *International Journal of Circuit Theory and Applications*, vol. 38, no. 6, pp. 649-659, 2010.

[5] E. Tlelo-Cuautle, Sánchez-López, E. Martinez-Romero, Sheldon X.-D. Tan, Symbolic analysis of analog circuits containing voltage mirrors and current mirrors, *Analog Integrated Circuits and Signal Processing*, vol. 65, no. 1, pp. 89-95, 2010.

[6] D. De Jonghe, G. Gielen, Characterization of Analog Circuits Using Transfer Function Trajectories, *IEEE Transactions on Circuits and Systems I: Regular papers*, 2012. DOI: 10.1109/TCSI.2011.2180438

[7] M. Fakhfakh, E. Tlelo-Cuautle, F.V. Fernández, *Design of Analog Circuits through Symbolic Analysis*, Bentham Sciences Publishers Ltd., 2012.

[8] Guoyong Shi, A survey on binary decision diagram approaches to symbolic analysis of analog integrated circuits, *Analog Integrated Circuits and Signal Processing*, 2011. DOI: 10.1007/s10470-011-9773-8

[9] Santiago Rodriguez-Chavez, Esteban Tlelo-Cuautle, Adolfo A. Palma-Rodriguez, and Sheldon X.-D. Tan, *Symbolic DDD-based tool for the computation of noise in CMOS analog circuits*, International Caribbean Conference on Devices, Circuits and Systems (ICCDCS), Playa del Carmen, Mexico, March 14-17, 2012.

[10] Adolfo A. Palma-Rodriguez, Esteban Tlelo-Cuautle, Santiago Rodriguez-Chavez, and Sheldon X.-D. Tan, *DDD-Based Symbolic Sensitivity Analysis of Active Filters*, International Caribbean Conference on Devices, Circuits and Systems (ICCDCS), Playa del Carmen, Mexico, March 14-17, 2012.

[11] S. X.-D. Tan, X.-X. Liu, E. Mlinar, E. Tlelo-Cuautle, *Parallel Symbolic Analysis of Large Analog Circuits on GPU Platforms*, in VLSI Design, pp. 113-128, InTech Publisher, January 2012.

[12] R. Senani, S.S. Gupta, Current-Mode Universal Biquad Using Current Followers: A Minimal Realization, *Radioengineering*, vol. 20, no. 4, pp. 898-904, 2011.